Journal of Physics: Conference Series **544** (2014) 012021 doi:10.1088/1742-6596/544/1/012021

Topological stirring of two-dimensional atomic Bose-Einstein condensates

A. C. White[1,2], N. P. Proukakis[1] & C. F. Barenghi[1]

[1] Joint Quantum Centre (JQC), Durham-Newcastle, School of Mathematics and Statistics, Newcastle University, Newcastle upon Tyne, NE1 7RU, United Kingdom.

[2] School of Mathematical Sciences, University of Nottingham, University Park, Nottingham, NG7 2RD, United Kingdom.

E-mail: ang.c.white@gmail.com

Abstract. We stir vortices into a trapped quasi two-dimensional atomic Bose-Einstein condensate by moving three laser stirrers. We apply stirring protocols introduced by Boyland *et al.* (2000), that efficiently build in topological chaos in classical fluids and are classified as Pseudo-Anosov stirring protocols. These are compared to their inefficient mixing counterparts, finite-order stirring protocols. We investigate if inefficient stirring protocols result in a more clustered distribution of vortices. The efficiency with which vortices are 'mixed' or distributed in a condensate is important for investigating dynamics of continuously forced quantum turbulence and the existence of the inverse cascade in turbulent two-dimensional superfluids.

1. Introduction

Jupiter's Great Red Spot is a beautiful demonstration of a large spot of vorticity, one of the defining features of two dimensional (2D) classical turbulence, arising from the inverse cascade process (Sommeria *et al.* (1988); Marcus (1988)). This process describes the flow of energy from small scales, given by the scale at which energy is injected into the system, to larger scales, manifesting in the clustering of vortices of like-winding. The concept of an inverse energy cascade process was introduced by Onsager (1949), who showed that clusters of like-signed point vortices in a large Onsager gas of many point-vortices possess negative temperature. Quantum vortices in superfluid He can be realistically modelled as point vortices or vortex lines, due their small vortex core size ($\sim$ 1nm), quantised vorticity and large ratio of inter-vortex spacing to vortex core radius ($\sim 10^5 - 10^6$). At large scales greater than the average inter-vortex spacing, three dimensional turbulent quantum fluids are also known to exhibit the same classical Kolmogorov energy spectrum with scaling $k^{-5/3}$ (where k is the wavenumber) as classical fluids (see Nore *et al.* (1997); Maurer & Tabeling (1998); Stalp *et al.* (1999); Araki *et al.* (2002); Kobayashi & Tsubota (2005); Salort *et al.* (2010); Baggaley & Barenghi (2011) and Baggaley *et al.* (2012)). For these reasons, one might expect the inverse cascade process to occur in other two dimensional quantum fluids, such as Bose-Einstein condensates (BECs), where vortices also have quantised circulation. While at large scales turbulent quantum fluids are known to have similarities to turbulent classical fluids for three dimensional systems, for two dimensional systems such a crossover is yet to be established. There have been some numerical simulations working towards this goal in trapped and homogeneous condensates, however, to date there is no conclusive demonstration of the inverse cascade process for harmonically trapped atomic BECs (Parker

& Adams (2005); Horng *et al.* (2009); Numasato *et al.* (2010); Numasato & Tsubota (2010); White *et al.* (2012); Bradley & Anderson (2012); Reeves *et al.* (2012*a*,*b*)). Unlike in superfluid He, atomic BECs of low dimensions can be routinely created and manipulated experimentally and so they provide a promising system for such investigations. One important component of any two dimensional turbulent set-up is the introduction of vortices into the condensate in a controlled manner, such that their distribution is well-mixed. Finding such a well-mixed vortex distribution will be the focus of this work.

Recently White *et al.* (2012) showed that the trajectory a single laser stirrer takes through the condensate determines if the resulting vortices are clustered or more randomly distributed. We found that a single laser moving on a circular trajectory creates an initial cluster of like-signed vortices. While the extent of clustering was found to increase with stirring, it did not persist and decayed after the laser stirrer was turned off. This clustering of vortices manifests due to the trajectory of the laser stirrer, and not as a result of an inverse cascade process. Indeed it was shown that altering the trajectory of the laser stirrer resulted in less-extensive clustering and vortices could even be created in more randomly distributed configurations. In this work we employ three laser stirrers and measure the distribution and clustering of vortices by applying statistical measures of clustering previously developed in White *et al.* (2012). In particular, we stir the condensate in a manner that is known to efficiently mix classical fluids, known as pseudo-Anosov stirring protocols. These are contrasted to finite-order stirring protocols which have been shown to be inefficient mixers for classical fluids.

In this paper we proceed in the following way. Firstly we give an overview of topological stirring protocols and then outline the model applied to simulate vortex dynamics in atomic BECs. Finally we introduce statistical measures of clustering that are applied to give insight into how two quite different stirring protocols influence vortex dynamics in a surprisingly similar way. While this is unexpected from the perspective of classical fluids, it is a remarkable demonstration of the potential flow of quantum fluids.

2. Topological stirring protocols

Topological concepts were introduced to address the question of how to most efficiently mix classical fluids. Boyland *et al.* (2000) determined that for flows with the topology of certain braids, given only the topology of the flow, it is possible to deduce the material stretch rate. For stokes flow (characterised by Reynolds number, $Re \ll 1$), chaotic advection of fluid particles is built into the flow faster by stirring schemes that build in topological chaos. Such protocols are classified as pseudo-Anosov stirring protocols and it is established that stirring a fluid in such a way results in exponential stretching of material lines. Stirring protocols that do not have the correct topology to mix effectively are known as finite-order stirring protocols (Boyland *et al.* (2000); Finn *et al.* (2003); Gouillart *et al.* (2006)). In classical fluids, finite-order stirring protocols have been shown to stretch material lines linearly and therefore do not mix as efficiently as their pseudo-Anosov counterparts.

The trajectory of the stirring lasers can be represented by braid-diagrams in space-time, with braid letters σ_i denoting the exchange of stirrers labelled i and $i+1$ in a clockwise direction. This can be depicted in a braid diagram by the strand corresponding to the stirrer labelled $i+1$ passing over the strand showing the ith stirrer. Similarly, an anti-clockwise path of stirrers through the condensate is denoted by braid letters σ_{-i} which represents stirrers $i+1$ and i exchanging position in an anti-clockwise direction. This interchange is shown on a braid-diagram by the strand depicting the $i+1$ stirrer passing under the ith strand. Figure 1 (A) illustrates the braid diagram corresponding to the exchange of stirrers following a protocol that can be classified as pseudo-Anosov.

Each stirring operation, corresponding to a braid letter, can be represented by a braid matrix. For the stirring operations corresponding to the σ_1, σ_{-1} and σ_2 braid letters, which we apply

in this work, the corresponding braid matrices take the form (Boyland *et al.* (2000); Finn *et al.* (2003))

$$\Sigma_1 = \begin{bmatrix} 1 & -1 \\ 0 & 1 \end{bmatrix}, \quad \Sigma_{-1} = \begin{bmatrix} 1 & 1 \\ 0 & 1 \end{bmatrix}, \quad \Sigma_2 = \begin{bmatrix} 1 & 0 \\ 1 & 1 \end{bmatrix}. \tag{1}$$

The time-like sequence of braid letters composes a braid word, where the rightmost letter gives the first stirring operation and the leftmost letter denotes the most recent stirring operation. We concentrate on two stirring protocols, which we label A and B that are represented by the braid words

$$A = (\sigma_1\sigma_2)^n \quad \text{and} \quad B = (\sigma_{-1}\sigma_2)^n \ , \tag{2}$$

here n denotes the number of repetitions of braid letter operations. Similarly, the corresponding action of the braid matrices takes the form

$$A = [\Sigma_1\Sigma_2]^n \quad \text{and} \quad B = [\Sigma_{-1}\Sigma_2]^n \ . \tag{3}$$

Stirring protocol A is a finite-order protocol, while protocol B is a pseudo-Anosov stirring protocol which builds topological chaos into the flow. The topology of the fluid flow is completely characterised by the braid word, regardless of the nature of the fluid flow, i.e. if it is compressible, incompressible, viscous or inviscid. For three stirrers, the magnitude of the largest eigenvalue of the associated braid matrix, called the spectral radius, gives a rate at which at least one material line is stretched. Finn *et al.* (2003) computed the stretching in time of a finite material line element and showed that the chaotic region of the fluid flow is of the same extent as the region of fluid the stirrers are moved through.

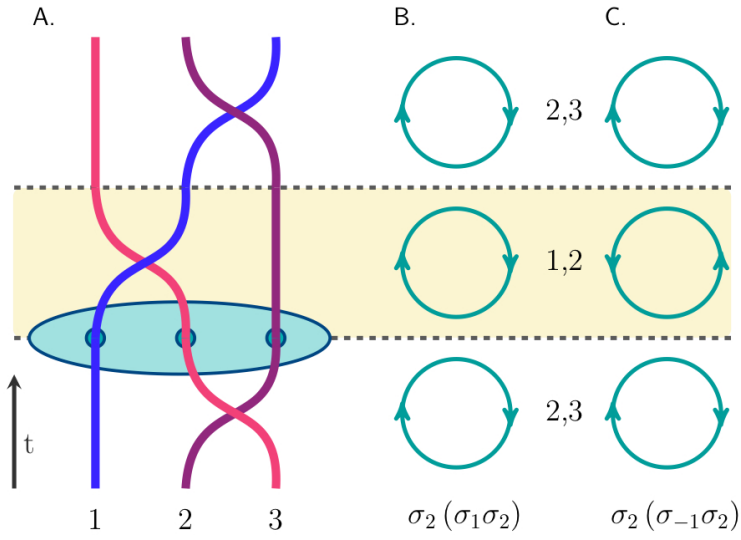

Figure 1. (A) Braid representation in space and time depicting the exchange of stirrers for a pseudo-Anosov stirring protocol. Three stirring operations are shown, corresponding to the exchange of stirrers $\sigma_2 = (2,3)$, then $\sigma_{-1} = (1,2)$ and again stirrers $\sigma_2 = (2,3)$. The rotation stirrers trace out are depicted in (B) for a finite-order stirring protocol and (C) for the pseudo-Anosov stirring protocol depicted in (A).

In the remainder of this paper we present numerical simulations of three laser stirrers in an atomic BEC tracing out the finite-order and pseudo-Anosov stirring schemes A and B, presented above. Note the stirrers trace out a figure eight path, depicted in figure 2. We choose the velocity of the laser stirrers to be larger than the critical velocity for vortex nucleation in order to determine if a pseudo-Anosov stirring protocol (B) also results in a more random distribution of vortices than a finite-order stirring scheme (A).

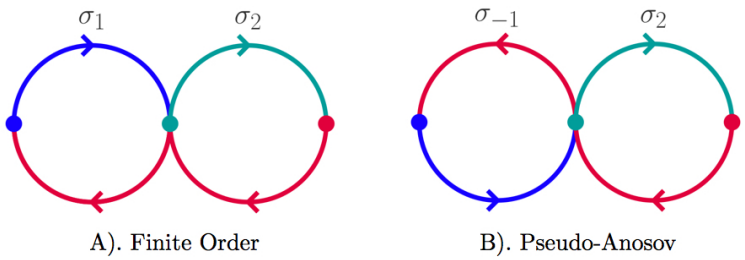

Figure 2. Stirrer paths for first two stirring operations of A) finite-order stirring protocol and B) pseudo-Anosov stirring protocol.

3. Modelling vortex dynamics

The second quantised hamiltonian describing a trapped, weakly-interacting atomic Bose-Einstein condensate takes the form

$$H = \int d\tilde{\mathbf{r}} \left[-\hat{\Psi}^\dagger(\tilde{\mathbf{r}}) \frac{\hbar^2}{2m} \nabla^2 \hat{\Psi}(\tilde{\mathbf{r}}) + (V(\tilde{\mathbf{r}}) + V_P) \hat{\Psi}^\dagger(\tilde{\mathbf{r}}) \hat{\Psi}(\tilde{\mathbf{r}}) + \frac{U_0}{2} \hat{\Psi}^\dagger(\tilde{\mathbf{r}}) \hat{\Psi}^\dagger(\tilde{\mathbf{r}}) \hat{\Psi}(\tilde{\mathbf{r}}) \hat{\Psi}(\tilde{\mathbf{r}}) \right] . \quad (4)$$

Here $\hat{\Psi}(\tilde{\mathbf{r}})^\dagger$ and $\hat{\Psi}(\tilde{\mathbf{r}})$ are the creation and annihilation operators for bosons of mass m, trapped in a potential $V(\tilde{\mathbf{r}})$. The laser stirrers are described by V_P. The boson-boson interaction is given by a contact potential $U_0 = 4\pi\hbar^2 a/m$, where a is the s-wave scattering length. The evolution of the field operator can be obtained from the Heisenberg equations of motion. At low temperatures, we can describe the condensed state by a classical mean field $\Psi = \langle\hat{\Psi}\rangle$ and excitations $\langle\phi\rangle$, decomposing the boson operators as $\hat{\Psi} = \Psi + \langle\phi\rangle$. The dynamics of the mean-field condensate wavefunction are then given by the nonlinear Schrödinger equation

$$i\hbar \frac{\partial \Psi(\tilde{\mathbf{r}})}{\partial \tilde{t}} = -\frac{\hbar^2}{2m} \nabla^2 \Psi(\tilde{\mathbf{r}}) + (V(\tilde{\mathbf{r}}) + V_P) \Psi(\tilde{\mathbf{r}}) + U_0 |\Psi(\tilde{\mathbf{r}})|^2 \Psi(\tilde{\mathbf{r}}) . \quad (5)$$

We consider a condensate trapped such that the axial trapping frequency is much greater than the radial trapping frequency, $\omega_z \gg \omega_r$. In this case the condensate is quasi-two dimensional. For our simulations we model the dimensionless form of the 2D non-linear Schrödinger equation,

$$i\frac{\partial \psi}{\partial t} = -\frac{1}{2}\nabla^2\psi + \frac{r^2}{2}\psi + V_P\psi + \kappa_{2d}|\psi|^2\psi . \quad (6)$$

Here the 2D interaction strength takes the form $\kappa_{2d} = 2\sqrt{2\pi}aN/a_z$, where N is the total number of atoms in the condensate. The 2D condensate wavefunction is written as $\psi = a_r\Psi/\sqrt{N}$ and we have imposed the normalisation $\int \mathrm{d}\mathbf{x}|\psi|^2 = 1$. The radial (axial) trapping frequency, ω_r (ω_z), determines the radial (axial) harmonic oscillator length $a_r = \sqrt{\hbar/(m\omega_r)}$ ($a_z = \sqrt{\hbar/(m\omega_z)}$). We choose the scaling for lengths and time to be $\tilde{r}/a_r = r$ and $\tilde{t}\omega_r = t$, where $\tilde{r}$ and $\tilde{t}$ are dimensional with units of meters and seconds respectively. We solve Eq.(6) pseudo-spectrally, applying an adaptive 4-5th order Runge-Kutta method in time (Dennis *et al.* (2013)). We select a stirring strength $V_0 \sim 2.6\mu$, where μ is the chemical potential of the BEC. We choose $\kappa = 10400$, which taking ^{23}Na atoms corresponds to parameters of $\omega_z = 2\pi \times 50$Hz, $\omega_r = 2\pi \times 5$Hz, $N = 2.2 \times 10^6$ and $a = 2.75$nm. Simulations are run on a 512^2 grid of spatial extent -20 to 20. Snap-shots of time-evolution of the condensate density profile is depicted in figure 3.

3.1. Decomposition of the Kinetic Energy contribution

For a time-independent potential, the total energy of the system is conserved within the nonlinear Schrödinger equation. Writing the mean-field condensate wavefunction in terms of the condensate density $n = |\psi|^2$, and phase θ, as $\psi = \sqrt{n}\exp[i\theta]$, the kinetic energy component

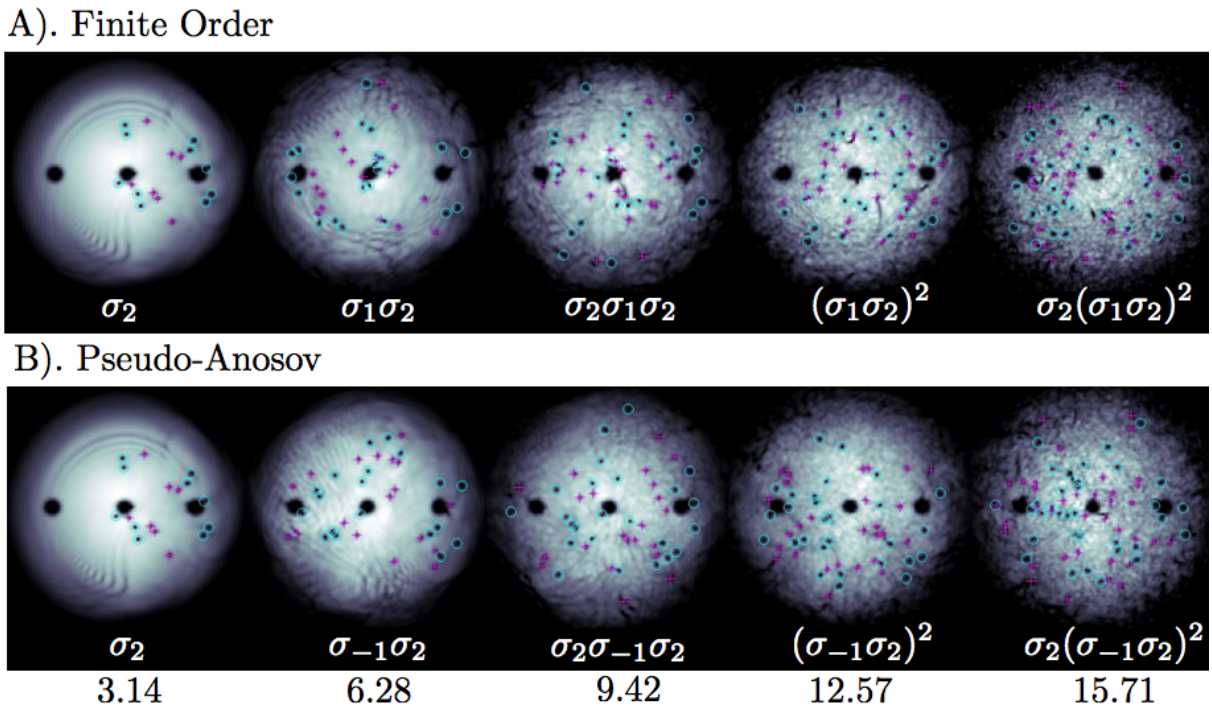

Figure 3. Vortex Dynamics: Condensate density profiles after simulation times given along the bottom of the figure. Magenta + and cyan − symbols denote vortices with positive and negative winding respectively. Row A.) finite-order stirring protocol at times corresponding to braid-words σ_2, $\sigma_1\sigma_2$, $\sigma_2\sigma_1\sigma_2$, $(\sigma_1\sigma_2)^2$ and $\sigma_2\,(\sigma_1\sigma_2)^2$. Row B.) corresponds to pseudo-Anosov stirring protocols at identical times, corresponding to braid words σ_2, $\sigma_{-1}\sigma_2$, $\sigma_2\sigma_{-1}\sigma_2$, $(\sigma_{-1}\sigma_2)^2$ and $\sigma_2\,(\sigma_{-1}\sigma_2)^2$.

of the total energy can be decomposed into contributions from the quantum pressure and kinetic energy density (Nore *et al.* (1997))

$$E_{\mathsf{KE}} = \int \mathrm{d}\mathbf{x} \left(\frac{1}{2}|\nabla\psi|^2\right) = \int \mathrm{d}\mathbf{x} \left(\frac{1}{2}|\nabla\sqrt{n}|^2 + \frac{1}{2}|\sqrt{n}\mathbf{v}|^2\right) . \tag{7}$$

Here we have defined the velocity field $\mathbf{v} = \nabla\theta$. The kinetic energy density contribution can be further decomposed into a compressible component for which the density weighted velocity field $\boldsymbol{\Upsilon} = \sqrt{n}\mathbf{v}$, satisfies $\nabla \times \boldsymbol{\Upsilon}^c = 0$ and an incompressible, divergence free component $\nabla \cdot \boldsymbol{\Upsilon}^i = 0$, such that $\boldsymbol{\Upsilon} = \boldsymbol{\Upsilon}^i + \boldsymbol{\Upsilon}^c$. The total compressible energy is a useful measure of the total sound in the system and the total incompressible kinetic energy gives the total kinetic energy of vortices

$$E^{i,c}_{\mathsf{KE}} = \frac{1}{2}\int \mathrm{d}\mathbf{x}\,\left|\boldsymbol{\Upsilon}^{i,c}\right|^2 . \tag{8}$$

One can subsequently define compressible and incompressible kinetic energy spectrums, however due to the small size of trapped atomic condensates, only a short range of length scales is accessible in these systems, in comparison to other 2D turbulent systems. Consequently, evaluating scaling exponents from such spectrums is of limited use and the derived scaling laws should be interpreted with care. We refrain from such an analysis here.

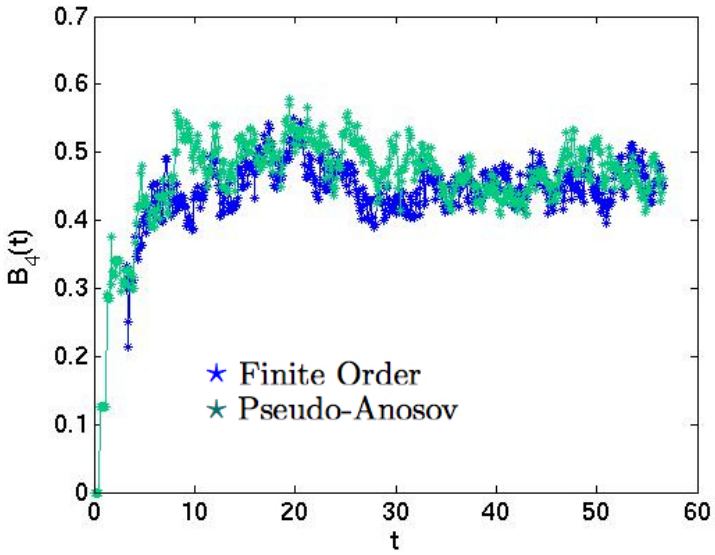

Figure 4. Evolution of vortex distribution statistics given by fourth nearest neighbor vortices for finite-order (blue $*$) and pseudo-Anosov (green $*$) stirring schemes.

3.2. Statistical measures of clustering

Motivated by the seminal work of Ripley (1976, 1977), White *et al.* (2012) developed statistical measures of clustering that are appropriate for measuring if vortices are clustered or more randomly distributed in atomic Bose-Einstein condensates. These measures have the advantage of being experimentally accessible as they rely only on knowledge of the position and winding of vortices, taking into account both the sign and distance between a reference vortex i and its neighbouring vortices j, up to its J^{th} nearest-neighbor,

$$B_J(t) = \frac{1}{N}\sum_{i=1}^{N}\sum_{j=1}^{J}\frac{b_{ij}(t)}{J}\,. \tag{9}$$

N denotes all vortices that are at a distance $d_i \geq R_E$ from the condensate edge. If vortex i and its j^{th} nearest neighbor are of opposite sign, $b_{ij} = 0$. If vortex i and its j^{th} nearest neighbor are of the same sign and separation distance between them, $d_{ij} \leq R_c$, then $b_{ij} = 1$. If vortex i and vortex j are separated by a distance larger than R_c, $(d_{ij} \geq R_c)$, then $b_{ij} = 0$. In this work we take the distance $R_c = R_E$ to be greater than the average inter-vortex separation distance and of the order of the largest cluster size. These constraints are included in the statistical measure of vortex distribution in Eq.(9), to account for edge effects that arise as we are dealing with a small system of finite size. The parameter limiting separation distance between vortices i and j gives a means to investigate the variation of clustering over spatial regions. We take vortex distribution to be clustered for values of $B_J(t) > 0.5$, while for more random vortex distributions $B_J(t) < 0.5$. Related measures of clustering have been recently applied to look at two dimensional turbulence in Bradley & Anderson (2012) and Reeves *et al.* (2012*b*).

4. Discussion and Conclusions

From the point of view of classical fluid dynamics, visualising and tracking the evolution of fluid material lines through the use of tracer particles such as dye, are standard and straightforward techniques that enable one to distinguish between underlying chaotic and regular dynamics in the fluid flow. For atomic Bose-Einstein condensates, the best method for flow visualisation is not so obvious, however some information about the condensate flow can be provided with current experimental techniques. The positions of vortices can be visualised through standard absorption imaging techniques and the condensate phase profile has the potential to be measured

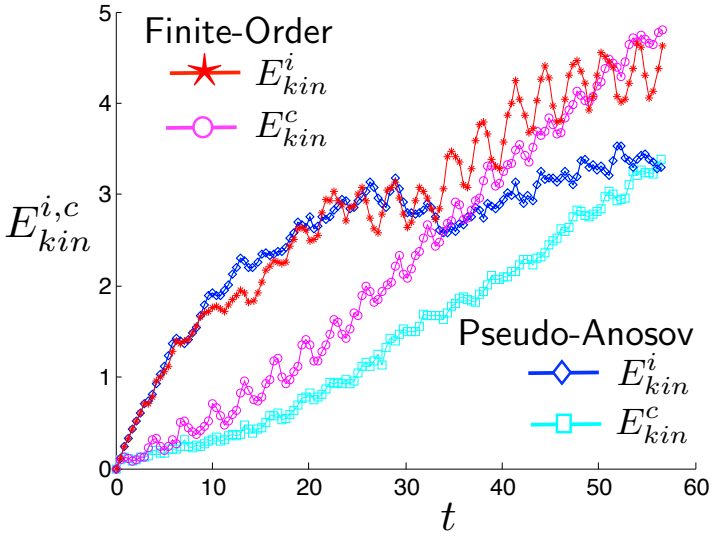

Figure 5. Incompressible and compressible kinetic energy distribution for finite-order stirring given by red stars and magenta circles respectively, and pseudo-Anosov stirring, given by blue diamonds and cyan squares respectively.

by applying interferometric measurements giving information about vortex winding. For these reasons we employ the statistical measure of clustering introduced above to analyse condensate flow.

We employ Eq.(9) up to fourth-nearest neighbor vortices and track the corresponding statistical measure of clustering, which is plotted in figure 4. Evidently, neither the finite-order nor the pseudo-Anosov stirring protocol that we have chosen results in a vortex distribution that is significantly clustered. After a few stirring operations, the vortices appear randomly distributed, independent of stirring protocol. This result is an indication of the potential nature of quantum fluids. One might expect underlying chaotic dynamics would result in a vortex distribution that is less clustered than underlying regular dynamics. Although material line elements are expected to be exponentially stretched for pseudo-Anosov stirring in contrast to the linear stretching of material line elements in the finite-order case, this does not appear to influence the vortex distribution. In other words, the vortex distribution is independent of if topological chaos is built into the flow by the method of stirring.

Another explanation for our observations may also lie in the speed at which the condensate is stirred. From a classical fluid perspective, when a container of classical fluid, such as water is stirred with very fast moving obstacles, the fluid will become turbulent and well-mixed, independent of the motion of the stirring obstacles provided their paths traverse a significant extent of the container surface. In this limit linear or exponential stretching of material line elements in the fluid may be present, but not visible. For a quantum fluid we can define limits on the speed at which the condensate is stirred. The lower limit on stirring speed is given by the condensate critical velocity, below which an obstacle moving through the condensate will not nucleate vortices. The upper limit is set by the speed at which fragmentation of the condensate occurs (Parker & Adams (2005)). In our simulations the condensate is stirred at speeds faster than the critical velocity for vortex nucleation, but not so fast that we enter the regime of condensate fragmentation. Although the speed of stirring is chosen to be fast enough to nucleate vortices, this does not necessarily imply we are in the quantum analogue of the classical scenario described above, where linear or exponential stretching of material lines may be present but not visible due to the very fast stirring speeds. Defining the analogue of such a limit is an interesting question we leave for future work.

From the analysis of the incompressible and compressible kinetic energy distribution (see figure 5), it is found that pseudo-Anosov stirring results in less sound being generated in

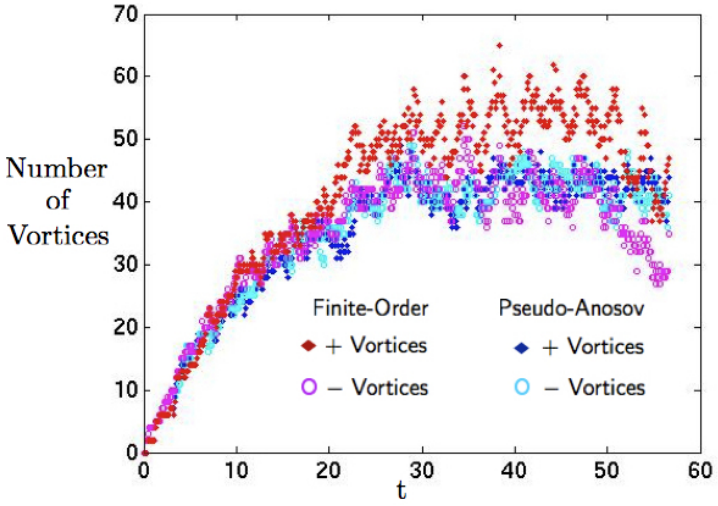

Figure 6. Evolution of number of vortices with positive and negative winding given by red diamonds and magenta circles respectively for finite-order stirring and blue diamonds and blue circles respectively for pseudo-Anosov stirring.

comparison to finite-order stirring protocols. The finite-order stirring scheme creates more sound in the condensate as result of the abrupt change in stirring direction during sequential stirring operations in this scheme. Although stirrers in both schemes follow trajectories that trace out a figure of eight shape, such abrupt changes in stirring direction do not occur in the pseudo-Anosov stirring scheme employed. Although at times $t < 30$ the total incompressible kinetic energy is initially similar for both stirring protocols, at later times more incompressible kinetic energy is generated for finite-order stirring. This difference is also reflected in the total vortex number for both stirring protocols (refer to figure 6). Finite-order stirring generates a larger imbalance in the total number of positive and negative vortices than pseudo-Anosov stirring. The oscillations in the vortex number and kinetic energy distribution for finite order stirring reflect the oscillations in the total condensate volume induced by this stirring protocol.

In conclusion, we have applied both pseudo-Anosov and finite-order stirring protocols to introduce vortices in a quasi-two dimensional Bose-Einstein condensate. Efficient mixing, as described by exponential stretching of material lines, could be thought to also translate into efficient vortex mixing. However, we observe that for a trapped inhomogeneous Bose-Einstein condensate, there is no appreciable increase in 'mixing' of vortices, as determined by the random, or clustered nature of the vortex distribution. That is, we do not find any significant correlation between if topological chaos is being introduced into the flow and how random the resulting vortex distribution is. In future work, we set up a stirring scheme that induces topological chaos in three dimensional quantum fluid flow and also analyse the onset of chaos for both finite-order and pseudo-Anosov stirring schemes.

Acknowledgments

We thank the anonymous reviewer for their insightful comments and especially for raising the alternative explanation for our observations we have discussed. This work was supported by the EPSRC. ACW acknowledges funding from EPSRC grant No. EP/H027777/1 and CFB and NPP acknowledge funding from EPSRC grant No. EP/I019413/1.

References

Araki, T., Tsubota, M. & Nemirovskii, S. K. 2002 Energy spectrum of superfluid turbulence with no normal–fluid component. *Phys. Rev. Lett.* **89**, 145301.

Baggaley, A. W. & Barenghi, C. F. 2011 Quantum turbulent velocity statistics and quasiclassical limit. *Phys. Rev. E* **84**, 067301.

Baggaley, A. W., Laurie, J. & Barenghi, C. F. 2012 Vortex-density fluctuations, energy spectra, and vortical regions in superfluid turbulence. *Phys. Rev. Lett.* **109**, 205304.

Boyland, P. L., Aref, H. & Stremler, M. A. 2000 Topological fluid mechanics of stirring. *J. Fluid Mech.* **403**, 277.

Bradley, A. S. & Anderson, B. P. 2012 Energy Spectra of Vortex Distributions in Two-Dimensional Quantum Turbulence. *Phys. Rev. X* **2**, 041001.

Dennis, G. R., Hope, J. J. & Johnsson, M. T. 2013 Xmds2: Fast, scalable simulation of coupled stochastic partial differential equations. *Computer Physics Communications* **184** (1), 201 – 208.

Finn, M. D., Cox, S. M. & Byrne, H. M. 2003 Topological chaos in inviscid and viscous mixers. *J. Fluid Mech.* **493**, 345.

Gouillart, E., Thiffeault, J.-L. & Finn, M. D. 2006 Topological mixing with ghost rods. *Phys. Rev. E* **73**, 036311.

Horng, T.-L., Hsueh, C.-H., Su, S.-W., Kao, Y.-M. & Gou, S.-C. 2009 Two-dimensional quantum turbulence in a nonuniform Bose-Einstein condensate. *Phys. Rev. A* **80**, 023618.

Kobayashi, M. & Tsubota, M. 2005 Kolmogorov Spectrum of Superfluid Turbulence: Numerical Analysis of the Gross-Pitaevskii Equation with a Small-Scale Dissipation. *Phys. Rev. Lett.* **94**, 065302.

Marcus, P. S. 1988 Numerical simulation of Jupiter's great red spot. *Nature* **331**, 693.

Maurer, J. & Tabeling, P. 1998 Local investigation of superfluid turbulence. *Europhys. Lett.* **43**, 29.

Nore, C., Abid, M. & Brachet, M. E. 1997 Kolmogorov Turbulence in Low-Temperature Superflows. *Phys. Rev. Lett.* **78**, 3896.

Numasato, R. & Tsubota, M. 2010 Possibility of inverse energy cascade in two-dimensional quantum turbulence. *J. Low Temp. Phys.* **158**, 415.

Numasato, R., Tsubota, M. & L'vov, V. S. 2010 Direct energy cascade in two-dimensional compressible quantum turbulence. *Phys. Rev. A* **81**, 063630.

Onsager, L. 1949 *Nuovo Cimento (suppl.)* **6**, 279.

Parker, N. G. & Adams, C. S. 2005 Emergence and decay of turbulence in stirred atomic Bose-Einstein condensates. *Phys. Rev. Lett.* **95**, 145301.

Reeves, M. T., Anderson, B. P. & Bradley, A. S. 2012*a* Classical and quantum regimes of two-dimensional turbulence in trapped Bose-Einstein condensates. *Phys. Rev. A* **86**, 053621.

Reeves, M. T., Billam, T. B., Anderson, B. P. & Bradley, A. S. 2012*b* Inverse Energy Cascade in Forced 2D Quantum Turbulence ArXiv:1209.5824 [cond-mat.quant-gas].

Ripley, B. D. 1976 The second-order analysis of stationary point processes. *Biophysical Journal* **13**, 255.

Ripley, B. D. 1977 Modelling spatial patterns. *J. Royal. Stat. Soc. B* **39**, 172.

Salort, J., Baudet, C., Castaing, B., Chabaud, B., Daviaud, F., Dedelot, T., Diribarne, P., Dubrulle, B., Gagne, Y., Gauthier, F., Girard, A., Hébral, B., Rousset, B., Thibault, P. & Roche, P.-E. 2010 Turbulent velocity spectra in superfluid flows. *Phys. Fluids* **22**, 125102.

Sommeria, J., Meyers, S. D. & Swinney, H. L. 1988 Laboratory simulation of Jupiter's great red spot. *Nature* **331**, 689.

Stalp, S. R., Skrbek, L. & Donnelly, R. J. 1999 Decay of Grid Turbulence in a Finite Channel. *Phys. Rev. Lett.* **82**, 4831.

White, A. C., Barenghi, C. F. & Proukakis, N. P. 2012 Creation and characterization of vortex clusters in atomic Bose-Einstein condensates. *Phys. Rev. A.* **86**, 103635.